

Supporting Information

Cellular Carbon-Wrapped FeSe₂ Nanocavities with Ultrathin Walls and Multiple Rooms for Ion Diffusion-Confinement Ultrafast Sodium Storage

Yongchao Tang,^a Zongbin Zhao,*^a Xiaojuan Hao,^c Yue Wei,^d Han Zhang,^a Yanfeng Dong,^a Yuwei Wang,^a Xin Pan,^b Yanan Hou,^a Xuzhen Wang^b and Jieshan Qiu*^a

^a State Key Lab of Fine Chemicals, Liaoning Key Lab for Energy Materials and Chemical Engineering, School of Chemical Engineering, Dalian University of Technology, Dalian 116024, P. R. China

^b School of Chemistry, Dalian University of Technology, Dalian 116024, China

^c Manufacturing, Commonwealth Scientific and Industrial Research Organization (CSIRO), Clayton, VIC 3168, Australia

^d State Key Laboratory of Fine Chemicals, School of Chemical Engineering, Dalian University of Technology, Dalian 116024, Liaoning, China

*Corresponding authors: zbzha@dlut.edu.cn; jqiu@dlut.edu.cn

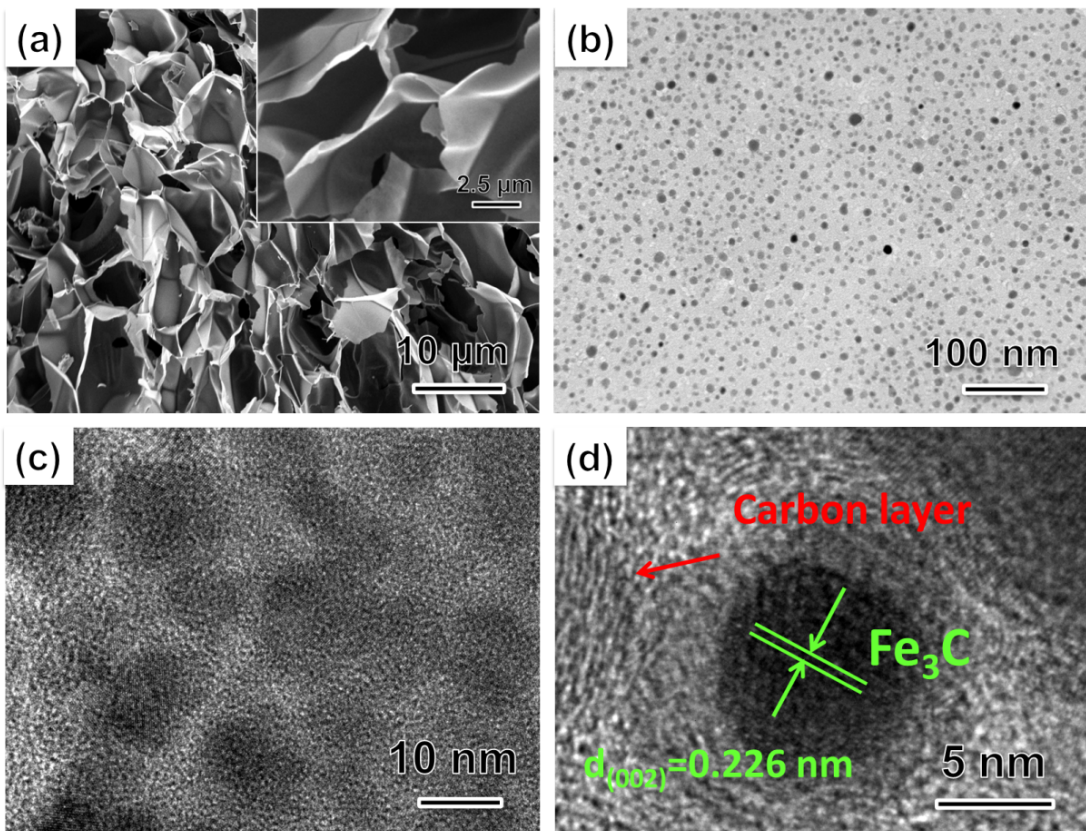


Figure S1. Morphological characteristic of Fe₃C@PC: (a) FE-SEM image featuring a typical cellular architecture constructed from smooth carbon sheets; (b) TEM image showing a uniform mosaic of Fe₃C nanoparticles; (c-d) HR-TEM images displaying the presence of carbon layers housing the Fe₃C nanoparticles.

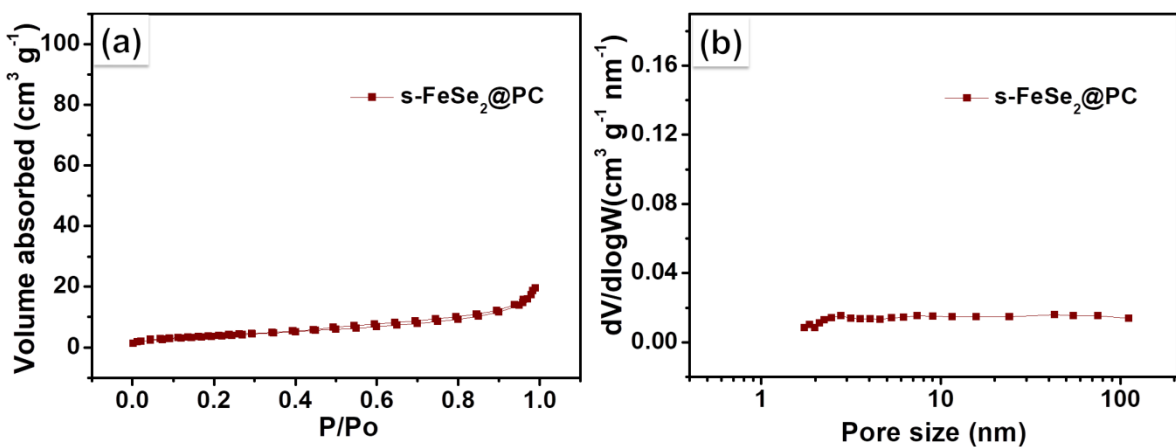


Figure S2. (a) N₂ adsorption isotherms of s-FeSe₂@PC and (b) the corresponding pore size distribution.

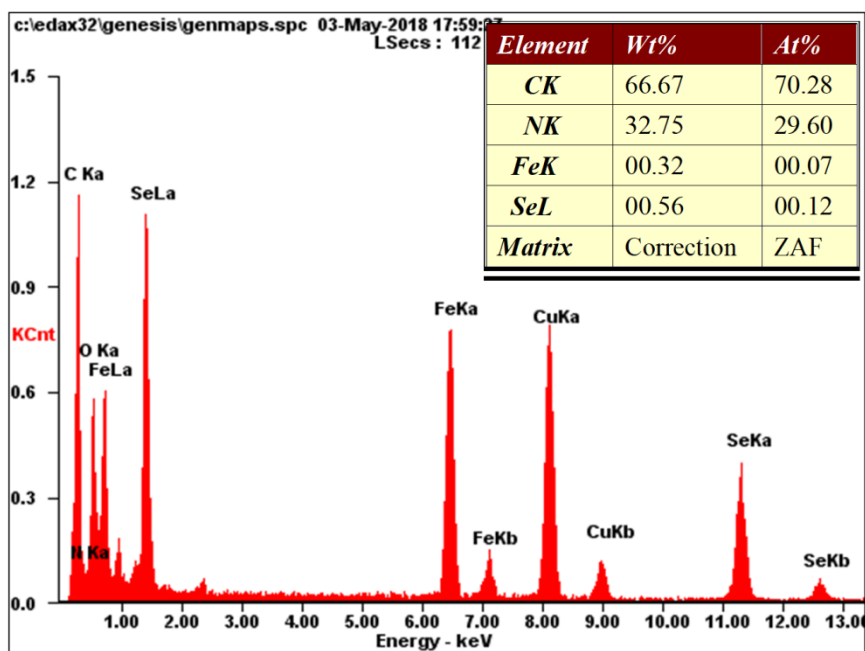


Figure S3. EDS spectra and corresponding elemental distribution of the as-obtained h-FeSe₂@PC.

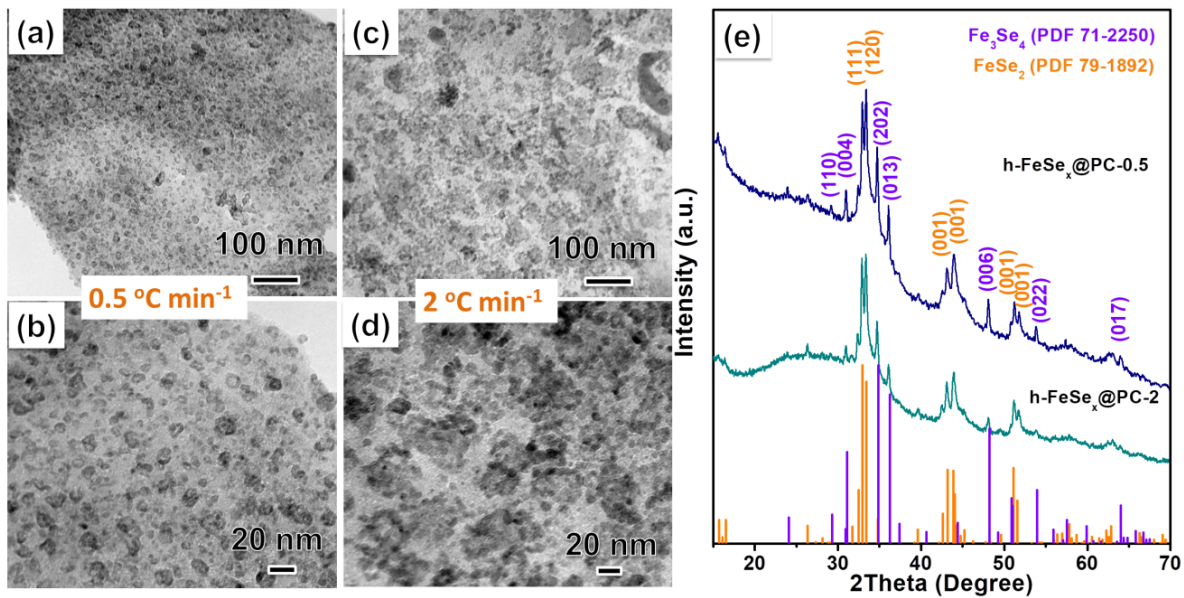


Figure S4. Chemical compositions and morphological features of samples obtained at different selenization ramp rates (0.5 and $2\text{ }^{\circ}\text{C min}^{-1}$): (a-b) XRD patterns of FeSe_x@PC-0.5 and FeSe_x@PC-2; (c-d) TEM images of FeSe_x@PC-0.5; (e-f) TEM images of FeSe_x@PC-2.

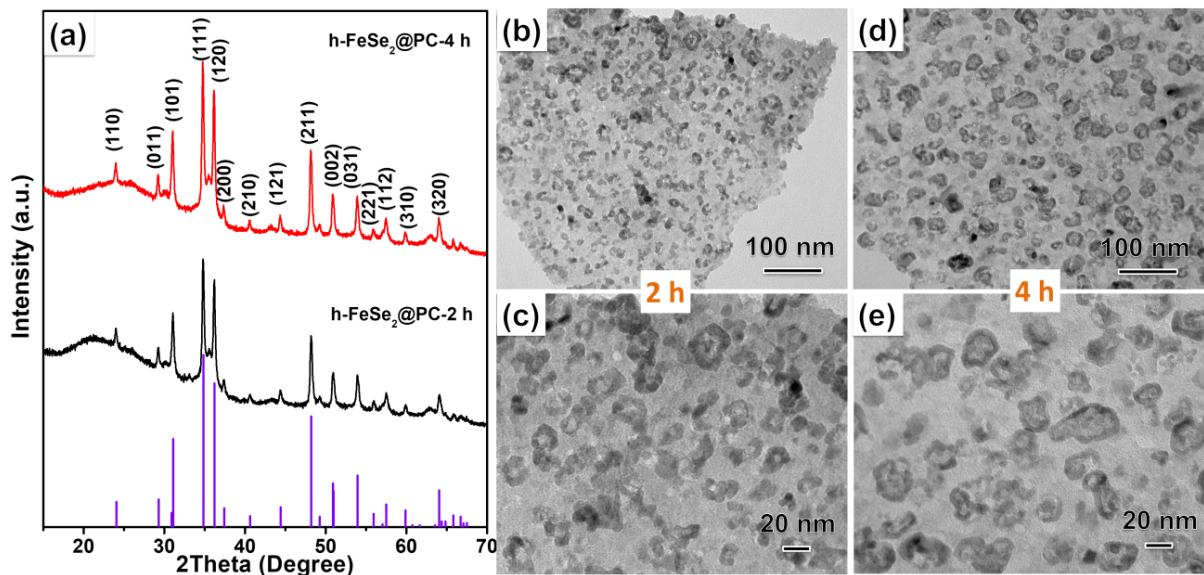


Figure S5. Morphological features and chemical compositions analysis of h-FeSe₂@PC with different selenization time showing the evolution of FeSe₂ nanocavities: (a) XRD patterns of h-FeSe₂@PC-2 and h-FeSe₂@PC-4; (b-c) TEM images of h-FeSe₂@PC-2 (2 h); (d-e) TEM images of h-FeSe₂@PC-4 (4 h).

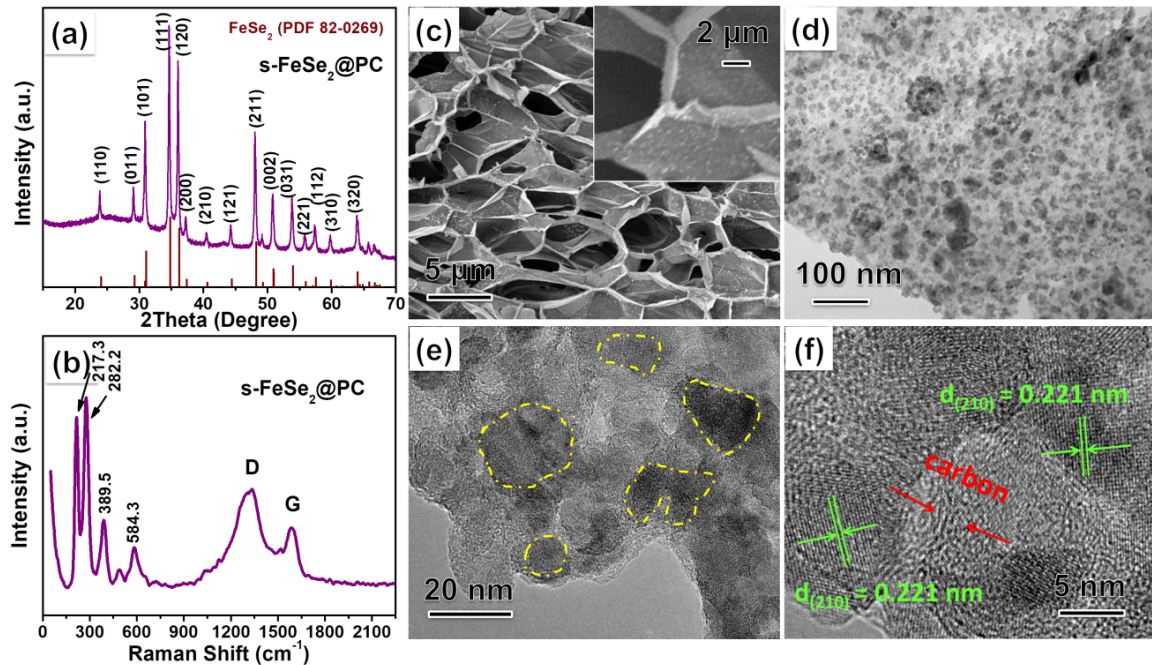


Figure S6. Chemical compositions and morphological features of s-FeSe₂@PC: (a) XRD pattern; (b) Raman spectrum; (c) FE-SEM images; (d-e) TEM images; (f) HR-TEM image.

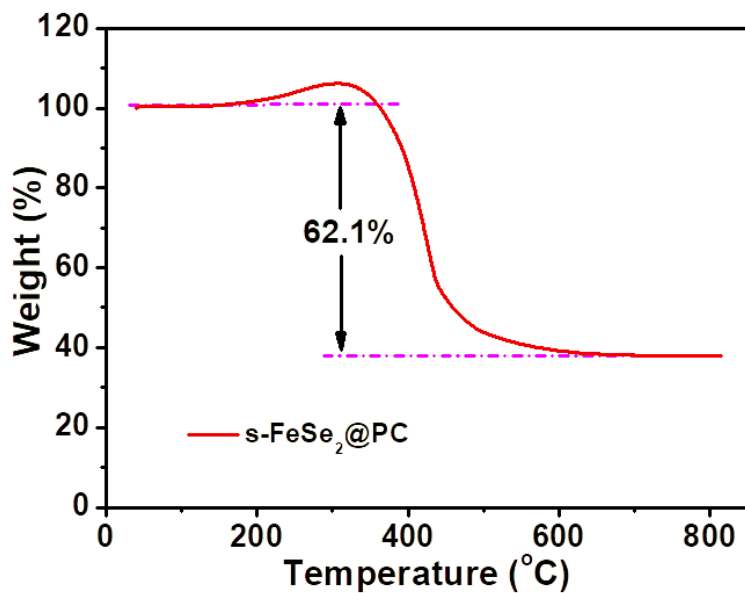


Figure S7. TGA profile of s-FeSe₂@PC showing around 62.1wt% weight loss.

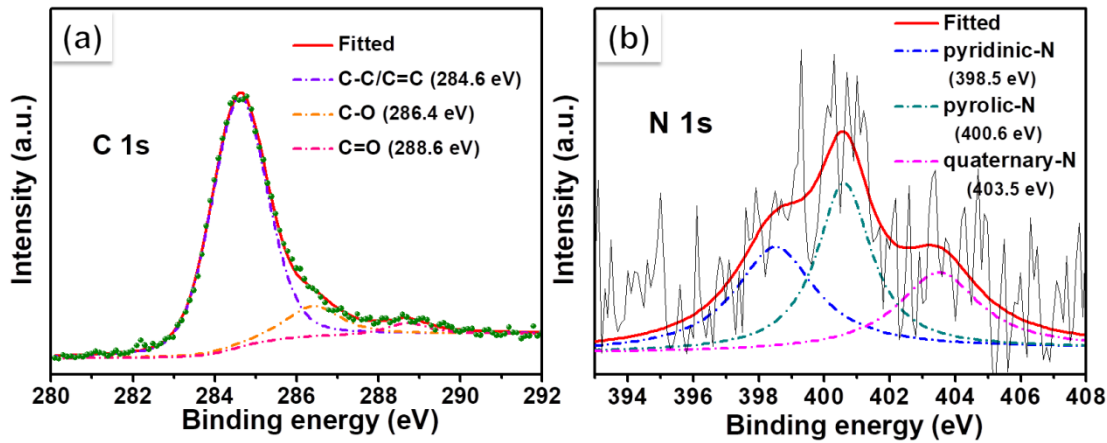


Figure S8. High resolution C 1s (a) and N 1s (b) XPS spectra in h-FeSe₂@PC.

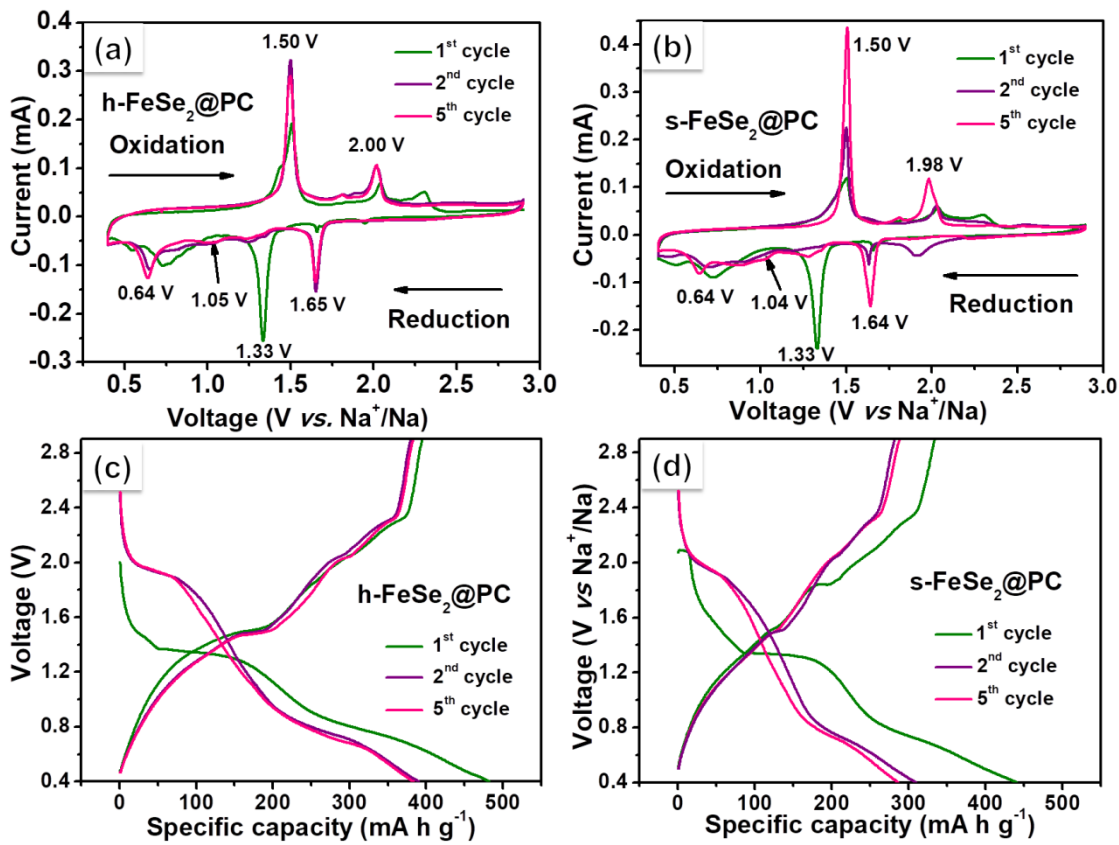


Figure S9 (a-b) CV curves of h-FeSe₂@PC and s-FeSe₂@PC anodes at a scan rate of 0.1 mV s⁻¹; (c-d) discharge/charge profiles of h-FeSe₂@PC and s-FeSe₂@PC anodes corresponding to (a) and (b), respectively.

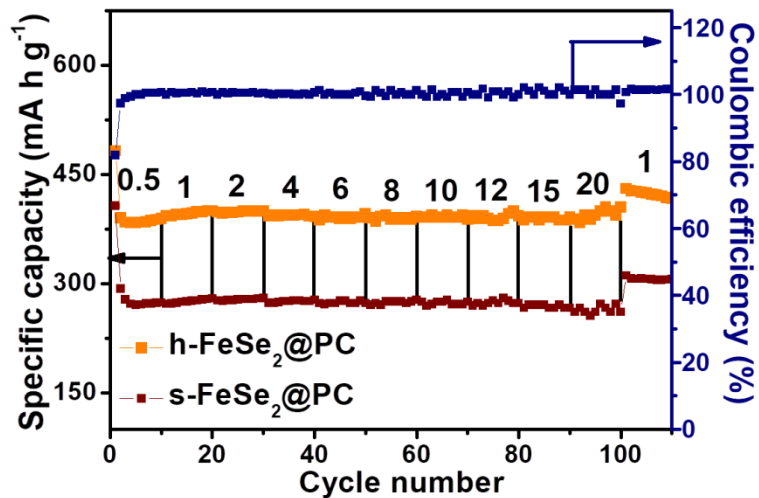


Figure S10. Rate capability of fresh h-FeSe₂@PC anode showing an ascending tendency of capacity with the increased current densities.

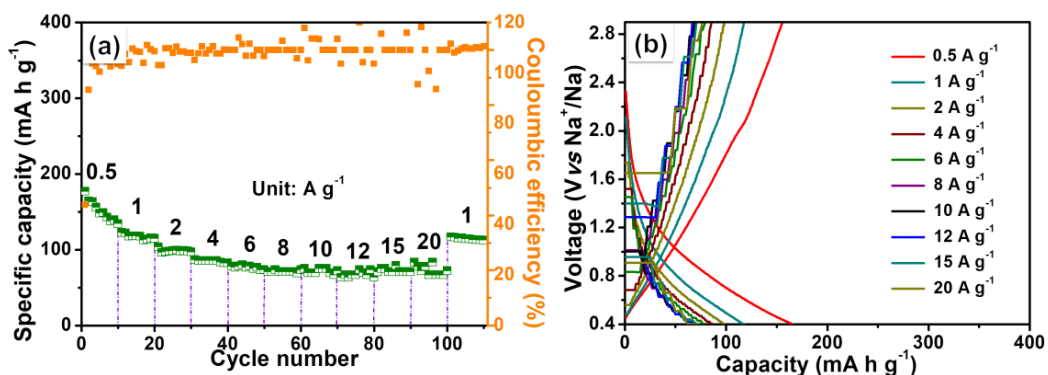


Figure S11. Electrochemical performance of PC anodes: (a) rate capability; (b) discharge/charge profiles at different current densities.

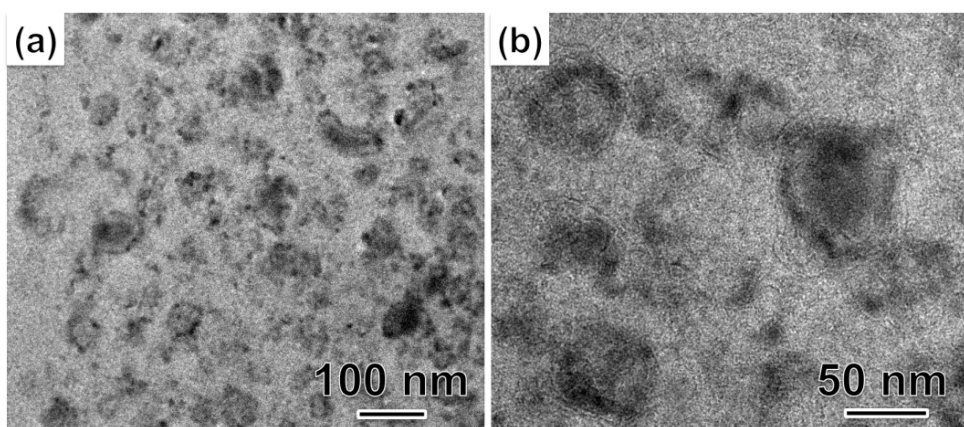


Figure 12. TEM images of the tested h-FeSe₂@PC anode at 5 A g⁻¹ over 2000 cycles.

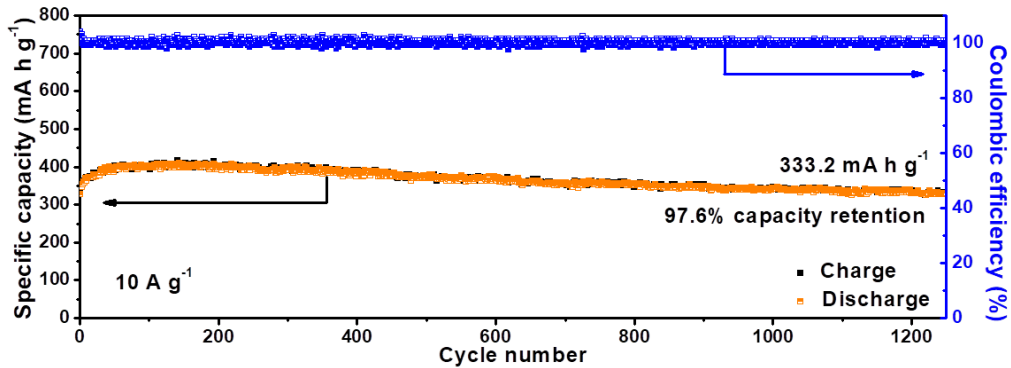


Figure S13. Long-life cyclability of h-FeSe₂@PC anode at 10 A g^{-1} over 1250 loops.

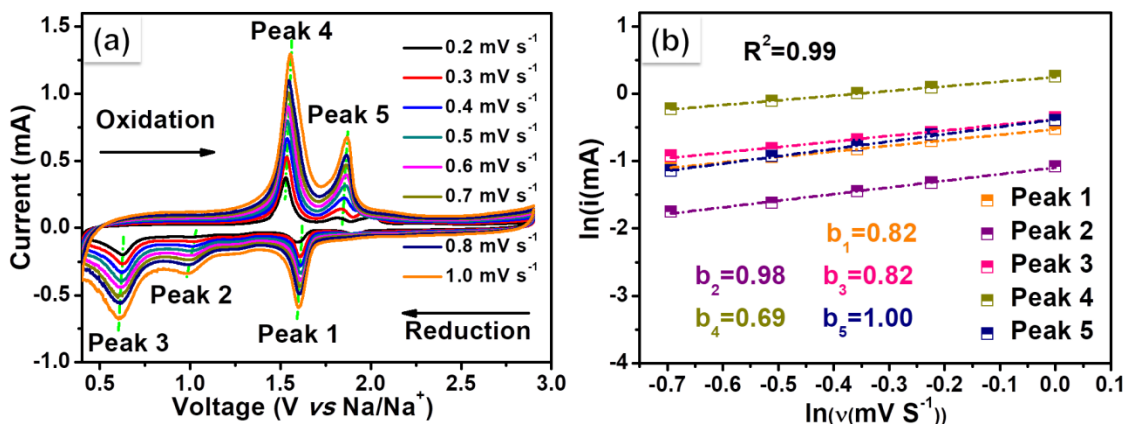


Figure S14. (a) CV curves and (b) corresponding b-values obtained from linear relationship between $\ln(i$ (peak current)) and $\ln(v$ (scan rate)).

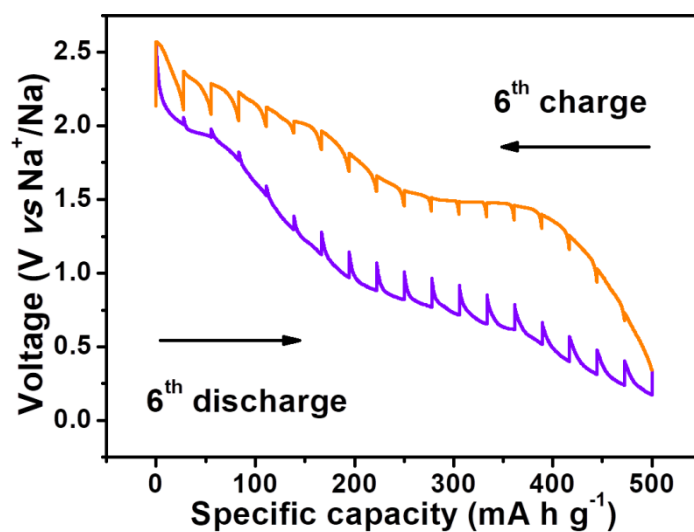


Figure S15. GITT curves of h-FeSe₂@PC anode at a pulse current density of 0.05 A g^{-1} .

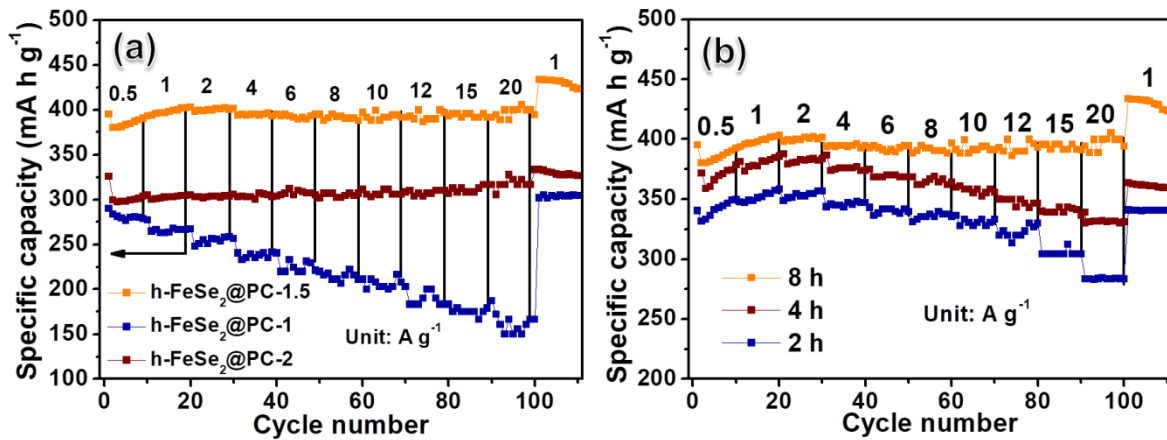


Figure S16. (a) Rate capability comparison of h-FeSe₂@PC samples with different FeSe₂ contents (where the number represents the mass ratio of PVP to Fe(NO₃)₂·9H₂O in chelated precursors); (b) rate capability comparison of h-FeSe₂@PC obtained with different selenization time (2, 4, 8 h).

Table S1. Rate capability comparison of various metal chalcogenide-based anodes with ether-based electrolyte.

Current density	Our work	CoS/RGO ¹	FeSe ₂ microspheres ²	Urchin-like CoSe ₂ ³	SnSSe ⁴	FeS ₂ @FeSe ₂ ⁵	CoSe@CSs ⁶	VS ₂ ⁷
(A g ⁻¹)	Specific capacity (mA h g ⁻¹)							
0.1		636	447	434		596	900	540
0.2				422			711	539
0.5	414.5	549	418	403		486	644	470
1	413.3	455	403	397	475	426	584	440
2	407.6	420		390			535	420
2.5					415			
4	400.2							
5		359	388	378	320	346	390	400
6	398.6							
7.5				226				
8	397.7						286	
10	395.5	306	337	354	161	203		353
12	393.0							
15	392.7			270				300
20	384.3		231	210				277
25			226					
30				163				

References

- [1] S. Peng, X. Han, L. Li, Z. Zhu, F. Chen, M. Srinivansan, S. Adams, S. Ramakrishna, *Small*, 2016, **12**, 1359-1368.
- [2] K. Zhang, Z. Hu, X. Liu, Z. Tao, J. Chen, *Adv. Mater.*, 2015, **27**, 3305-3309.
- [3] K. Zhang, M. Park, L. Zhou, G. Lee, W. Li, Y. Kang, J. Chen, *Adv. Funct. Mater.*, 2016, **26**, 6728-6735.
- [4] X. Wang, D. Chen, Z. Yang, X. Zhang, C. Wang, J. Chen, X. Zhang, M. Xue, *Adv. Mater.*, 2016, **28**, 8645-8650.
- [5] W. Zhao, C. Guo and C. M. Li, *J. Mater. Chem. A*, 2017, **5**, 19195-19202.
- [6] Z. Ali, T. Tang, X. Huang, Y. Wang, M. Asif and Y. Hou, *Energy Storage Materials*, 2018, **13**, 19-28.
- [7] R. Sun, Q. Wei, J. Sheng, C. Shi, Q. An, S. Liu and L. Mai, *Nano Energy*, 2017, **35**, 396-404.